ENGINEERING

# Sulfated polysaccharide directs therapeutic angiogenesis via endogenous VEGF secretion of macrophages

**Yuanman Yu[1], Kai Dai[1], Zehua Gao[2], Wei Tang[3], Tong Shen[2], Yuan Yuan[2], Jing Wang[1]*, Changsheng Liu[2]***



**Notwithstanding the remarkable progress in the clinical treatment of ischemic disease, proangiogenic drugs mostly suffer from their abnormal angiogenesis and potential cancer risk, and currently, no off-the-shelf biomaterials can efficiently induce angiogenesis. Here, we reported that a semisynthetic sulfated chitosan (SCS) readily engaged anti-inflammatory macrophages and increased its secretion of endogenous vascular endothelial growth factor (VEGF) to induce angiogenesis in ischemia via a VEGF-VEGFR2 signaling pathway. The depletion of host macrophages abrogated VEGF secretion and vascularization in implants, and the inhibition of VEGF or VEGFR2 signaling also disrupted the macrophage-associated angiogenesis. In addition, in a macrophage-inhibited mouse model, SCS efficiently helped to recover the endogenous levels of VEGF and the number of CD31$^{hi}$Emcn$^{hi}$ vessels in ischemia. Thus, both sulfated group and pentasaccharide sequence in SCS played an important role in directing the therapeutic angiogenesis, indicating that this highly bioactive biomaterial can be harnessed to treat ischemic disease.**

## INTRODUCTION

Reconstruction of the microvascular networks in ischemia is a fundamental challenge for tissue engineering (*1*). Numerous efforts have aimed to facilitate microvascular circulation to promote the growth of functional blood vessels like arterioles and sinusoids that functionally reconnect oxygen supplies and nutrient transportation via blood flow to a damaged area and alleviate hypoxia-induced cell death within implants (*2*–*4*). However, most efforts to date have focused primarily on exogenous growth factors and vascular cells. Recombinant angiogenic growth factors are not cost-effective and commonly associated with inappropriate blood vessel growth (*5*), while prevascularized implants cannot easily form anastomoses with host vasculature (*6*). In addition, as a previously unidentified technique, genetic modifications of transported cells to express angiocrine factors or antiapoptotic proteins are difficult to implement due to regulatory concerns (*7*). Thus, no effective strategies to restore the microvascular circulation of implants have reached mainstream clinical practice.

Accumulated evidences suggested that host cells like mesenchymal stem cells (*8*), osteoblasts (*9*), and preosteoclasts (*10*) could efficiently secrete growth factors to induce angiogenesis, while the biophysical effects of implanted materials on the regulation of biological activity of host cells are receiving more attention (*11*). Implants inherently elicit the accumulation of immune cells in vivo (*12*), while macrophages (Mφs) are required in immunoregulation and have been shown to function directly in angiogenesis (*13*, *14*). However, uncontrolled activation of Mφs causes an acute inflammatory response and leads to the formation of granulation tissue, hindering the ingrowth of new blood vessels and recovery of injury. The contribution of Mφs regulated by biomaterials to angiogenesis and vascular heterogeneity is still unknown, especially for implanted biomaterials.

Glycosaminoglycans (GAGs) are heterogeneous polysaccharides ubiquitous in mammalian tissues that act as a natural reservoir of diverse growth factors (*15*). As a highly sulfated GAG, heparin (Hep) interacts with numerous proteins to regulate physiological and pathological processes including inflammation, blood coagulation, lipid metabolism, angiogenesis, and neural regeneration (*16*). The combination of heparin and angiogenic growth factors has achieved great efficacy in the treatment of ischemic injury (*17*, *18*). However, the well-known anticoagulant property of heparin has been an obstacle to its use as a bioactive therapy. To address these issues, we previously developed the heparin-like polysaccharide semisynthetic sulfated chitosan (SCS) with a high affinity for vascular endothelial growth factor (VEGF), which efficiently promoted angiogenesis with an aid of extremely low concentration of exogenous VEGF (*19*). However, how SCS stimulated host cells in vivo to secrete growth factors and regulated its angiogenic bioactivity is still unknown.

In this work, we tried to use the properties of the biomaterial itself to guide the host cells and sought to explain how bioactive materials affected the microenvironment and promoted in situ angiogenesis in ischemia. To this end, we examined the heterogeneous angiogenesis following treatment with SCS in a mouse model of hind limb ischemia. SCS induced abundant CD31$^{hi}$Emcn$^{hi}$ vessels (Type H) and arteries relative to natural sulfated polysaccharide heparin. In addition, SCS notably regulated Mφs polarization to M2 with an elevated secretion of endogenous VEGF. Depletion of Mφs led to a sharp decrease in VEGF secretion and a deficiency in neovascularization, confirming the crucial bridging role of Mφs. Using the biomaterial design, we can create an implant that significantly promoted the resuscitation of mature blood vessels after Mφs deficiency.

## RESULTS

### SCS promotes angiogenesis following ischemic injury in mice

The properties of SCS were verified by gel permeation chromatography, element analysis, two-dimensional (2D) nuclear magnetic resonance,

[1]The State Key Laboratory of Bioreactor Engineering, East China University of Science and Technology, Shanghai 200237, P. R. China. [2]Key Laboratory for Ultrafine Materials of Ministry of Education, East China University of Science and Technology, Shanghai 200237, P. R. China. [3]Shenzhen Key Laboratory of Nanobiomechanics, Shenzhen Institutes of Advanced Technology, Chinese Academy of Sciences, Shenzhen 518055, P. R. China.
*Corresponding author. Email: biomatwj@163.com (J.W.); liucs@ecust.edu.cn (C.L.)

and Fourier transform infrared spectroscopy (fig. S1, A to D). The morphology of SCS-coated gelatin sponge (SCS GS) was observed by scanning electron microscopy (fig. S1E). As gelatin sponge (GS) is electroneutral in physiological condition, we first evaluated the release kinetics of SCS from gelatin sponge. The results showed that SCS GS appeared an obvious burst release at the initial stage but manifested a stable liberation in the subsequent process (fig. S1F). In addition, we found that both gelatin sponge (Blank GS) and SCS GS were suitable for cell adhesion, and SCS GS had no obvious cell cytotoxicity (fig. S1, G to I).

To explore the regulation of SCS in response to neovascularization in vivo, we first implanted Blank GS and SCS GS in a mouse model of hind limb ischemia and tracked blood flow at implantation sites from 6 hours to 28 days after surgery (Fig. 1A). Saline injection was used as a control. Laser Doppler imaging revealed that occlusion of the femoral artery caused a 30 and 10% decrease of limb perfusion in the implanted site and paw, respectively (Fig. 1, B and C, and fig. S2A). Over time, the blood perfusion at the implanted site and paw was progressively increased. In contrast, SCS GS induced a higher level of perfusion than Blank GS and saline at both days 7

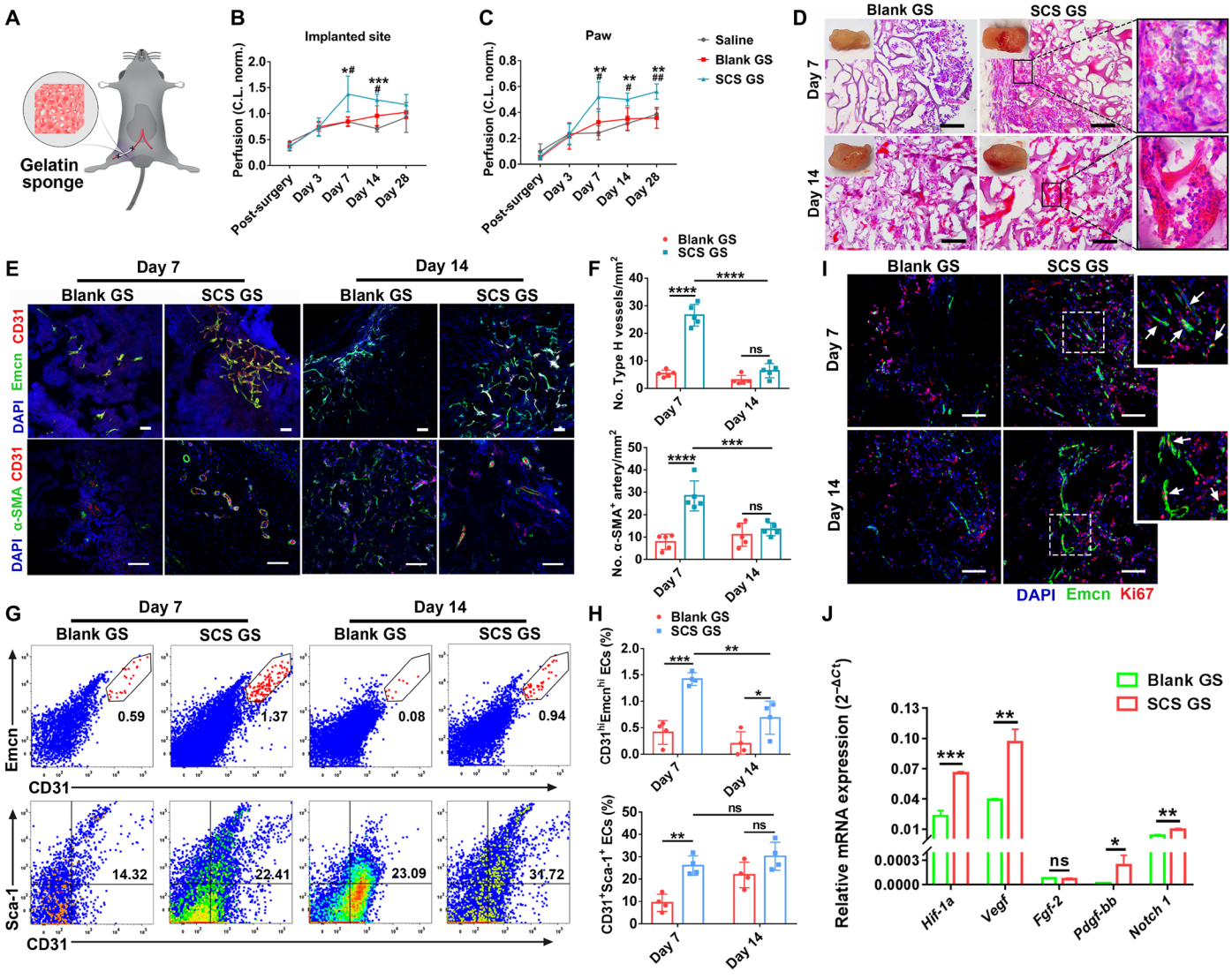


**Fig. 1. SCS promotes angiogenesis in hind limb ischemia.** (**A**) Illustration of mouse hind limb ischemia model (top left). (**B** and **C**) Quantification of perfusion levels of the implanted site (B) and paw (C) ($n = 4$). $^{*}P < 0.05$ versus saline; $^{\#}P < 0.05$ versus Blank GS. C.L. norm., contralateral (non-ischemic) limb normalized. (**D**) Hematoxylin and eosin (H&E) staining of implants on days 7 and 14 after implantation in ischemic limb. Insets are macroscopic views of the indicated implants. Photo credit: Y.Y., East China University of Science and Technology. (**E** and **F**) Representative immunostainings (E) with quantification (F) of CD31$^{hi}$Emcn$^{hi}$ (Type H) endothelium and α-SMA$^{+}$ arteries in Blank GS and SCS GS ($n = 5$). Scale bars, 100 μm. (**G** and **H**) Representative flow cytometry plots (G) with quantification (H) of CD31$^{hi}$Emcn$^{hi}$ and CD31$^{+}$Sca-1$^{+}$ endothelial cells ($n = 4$). (**I**) Representative images of endomucin (Emcn) and Ki67 immunostainings of proliferating cells ($n = 5$). White arrows, proliferating endothelial cells. Scale bars, 100 μm. (**J**) Relative angiogenic-related mRNA expressions of sorted CD31$^{+}$ endothelial cells from implants on day 7 ($n = 3$). Blank GS, gelatin sponge; SCS GS, SCS-coated gelatin sponge. Data are means ± SD. $^{*}P < 0.05$, $^{**}P < 0.01$, $^{***}P < 0.005$, and $^{****}P < 0.001$; $^{\#}P < 0.05$ and $^{\#\#}P < 0.01$; ns, not significant [(B) and (C), one-way analysis of variance (ANOVA) with Tukey's post hoc test; (F) and (H), two-way ANOVA with Tukey's post hoc test; (J), unpaired two-tailed Student's *t* test].

and 14, significantly restored perfusion of collateral circulation, and rescued the arterial perfusion in the ischemic hind limb.

To better understand how the SCS GS restored perfusion, we examined the vasculature of implants retrieved at days 7 and 14. SRμCT (Synchrotron radiation-based micro-computed tomography) angiography showed that relative blood vessel volume and vascular number were significantly higher in SCS GS than in Blank GS at days 7 and 14 (fig. S2, B to D). Moreover, the histology analysis showed that infiltration of microvessels and inflammatory cells was mainly concentrated on the periphery of both SCS GS and Blank GS at day 7, and microvessels and fibrous tissue were found to penetrate into the interior zone of implants at day 14 (Fig. 1D). A higher density of blood vessels and more mature vasculature with erythrocytes were observed in SCS GS compared to Blank GS.

We further investigated the vessel phenotypes generated in the implants. Endomucin (Emcn) was a sialoprotein expressed by non-arterial endothelial cells, while CD31 was highly expressed in arterial endothelial cells. $CD31^{hi}Emcn^{hi}$ endothelium (Type H), first found in the skeletal system, has the properties of high oxygenation and permeability, which has been associated with metabolic activity and osteogenesis (*20*). To address our hypothesis that Type H vessels are also generated in the ischemic repair system to achieve high-efficiency nutrient transfer and oxygen supply, we assessed $CD31^{hi}Emcn^{hi}$ endothelium levels in a mouse subcutaneous implant model and a mouse ischemic hind limb model. We found that no CD31 and Emcn double-positive endothelium was formed in the dorsal subcutaneous model with treatment of SCS GS (fig. S2, E to G). In contrast, a distinct Type H vessel was present in both implants in the ischemic hind limb model (a non-bone microenvironment) and was considerably higher in SCS GS than in Blank GS at day 7 (Fig. 1, E and F). However, the level of Type H vessels progressively decreased over time, and SCS GS exhibited no significant differences from Blank GS at day 14. We also found abundant arterial endothelial cells spontaneously organized into vascular networks that were stabilized with $\alpha$-$SMA^+$ ($\alpha$-smooth muscle actin–positive) cells in SCS GS at day 7 (Fig. 1, E and F) but decreased to a level comparable to Blank GS at day 14. Flow cytometry also confirmed greater amounts of $CD31^{hi}Emcn^{hi}$ endothelium cells and $CD31^+Sca\text{-}1^+$ arteriole cells in the SCS GS on day 7 after ischemic injury (Fig. 1, G and H).

Next, to better understand the function of new blood vessels, we examined the proliferative activity of endothelial cells and peripheral cells. As expected, SCS induced more proliferated endothelial cells in the implants versus Blank GS, and a high-density distribution of $Ki67^+$ proliferated cells was present around the vessels in the SCS GS (Fig. 1I). We next isolated the $CD31^+$ endothelial cells from implants at day 7 after hind limb ischemic injury. Treatment with SCS GS led to significant up-regulation of angiogenic-related mRNA (Fig. 1J). The expression of *Hif-1a*, *Vegf*, and *Notch 1* mRNAs was higher than that of *Fgf-2* and *Pdgf-bb* mRNAs.

To examine whether the in vivo degradation products of SCS were also involved in the regulation of angiogenesis in ischemia, we collected the implanted SCS GS at different time points after surgery and analyzed the components by high-performance liquid chromatography (HPLC). The results showed that the degradation products sulfated oligosaccharide (SCOS) appeared in abundance at day 14 after surgery (fig. S3A), which suggested that SCOS played a negligible role in inducing Type H vessels and arterioles. In addition, SCOS had no influences on cell viability of mouse peritoneal Mφs and could significantly promote the outgrowth of microvessels from arterial rings (fig. S3, B to D), which meant that the degradation of SCS had no harmful effects on the body. Together, these findings suggest that SCS significantly promotes the formation of Type H vessels and arteries and rescues the perfusion of ischemic hind limb, and its degradation does not involve in inducing angiogenesis.

## Sulfated group in polysaccharides functions in inducing angiogenesis

To further clarify which factor of SCS is essential in angiogenesis, we introduced three commercial polysaccharides—cationic polysaccharide [hydroxypropyltrimethyl ammonium chloride chitosan (HACC)], anion polysaccharide [carboxylated chitosan (CCS)], and heparin (Hep)—and analyzed their effects on angiogenesis. To investigate the effect of polysaccharide sequence on inducing Mφ-mediated angiogenesis, poly(styrenesulfonic acid sodium) (PSS) was also used. Elemental analysis revealed that SCS, Hep, and PSS exhibited a similar sulfur content, and $\zeta$ potential measurements confirmed the charge property of several polymers (Fig. 2A). The above results indicated that the Type H vessels and arteries were mainly generated after implantation for 7 days, so we chose this time point to compare the proangiogenic activity of polysaccharides. Immunostainings revealed that CCS GS and Hep GS recruited more $F4/80^+$ Mφs relative to other groups, and the Mφs in SCS GS exhibited a higher M1-to-M2 polarization capacity than others (fig. S4, A to D). In addition, we found that both SCS GS and Hep GS exhibited a similar degree of higher relative blood vessel volume and more ingrown endothelial cells relative to other groups (Fig. 2, B and C, and fig. S4E). Histology analysis demonstrated that both SCS GS and Hep GS promoted the ingrowth of microvessels. Specifically, we observed that CCS GS significantly inhibited the ingrowth of microvessels with the invasion of excess inflammatory cells (Fig. 2D).

We next investigated the effect of charged groups and polysaccharide sequence on the neovascular phenotype. Immunostainings showed that both non–saccharide sulfated polymer (i.e., PSS) and negatively charged polysaccharide (i.e., CCS) inhibited the formation of Type H vessels and arteries (Fig. 2, E to H). Hep GS could not efficiently stimulate the formation of Type H vessels compared to Blank GS (Fig. 2, E and F) but significantly induced arteriogenesis (Fig. 2, G and H). Enzyme-linked immunosorbent assay (ELISA) measurements revealed that both SCS GS and Hep GS significantly promoted the capture of endogenous VEGF (fig. S4F). Although previous studies have reported that negatively charged polymers were capable of binding to positively charged growth factors (*21*), we found that CCS GS could not efficiently capture VEGF via electrostatic interaction relative to SCS GS. In particular, PSS GS captured enough endogenous VEGF but failed to induce angiogenesis.

To further understand the regulation mechanism of the polymers on angiogenesis, the expression of mRNAs for secreted growth factors with known roles in endothelial cell survival and sprouting was analyzed in freshly isolated $CD31^+$ endothelial cells from implants. SCS GS expressed higher levels of *Hif-1a* and *Pdgf-bb* relative to Hep GS, while levels of *Vegf*, *Fgf-2*, and *Notch 1* were comparable (fig. S4, G to K). Likewise, *Hif-1a*, *Vegf*, and *Pdgf-bb* mRNA had significantly higher expression in SCS GS relative to PSS GS, CCS GS, and HACC GS. Next, we used Western blot analysis to study the effect of polymers on the VEGF receptor 2 (VEGFR2) signaling transduction of human umbilical vein endothelial cells (HUVECs)

A

| Sample | $M_w$ (Da) | Zeta potential (mV) | Sulfur content (%) |
|---|---|---|---|
| PSS | 17,000 | −18.4±2.7 | 12.5±0.3 |
| CCS | ~100,000 | −48.1±0.1 | – |
| HACC | ~100,000 | 66.4±2.6 | – |
| Hep | 20,000 | −52.7±1.4 | 11.4±0.4 |
| SCS | 15,394 | −50.6±1.1 | 12.4±0.1 |

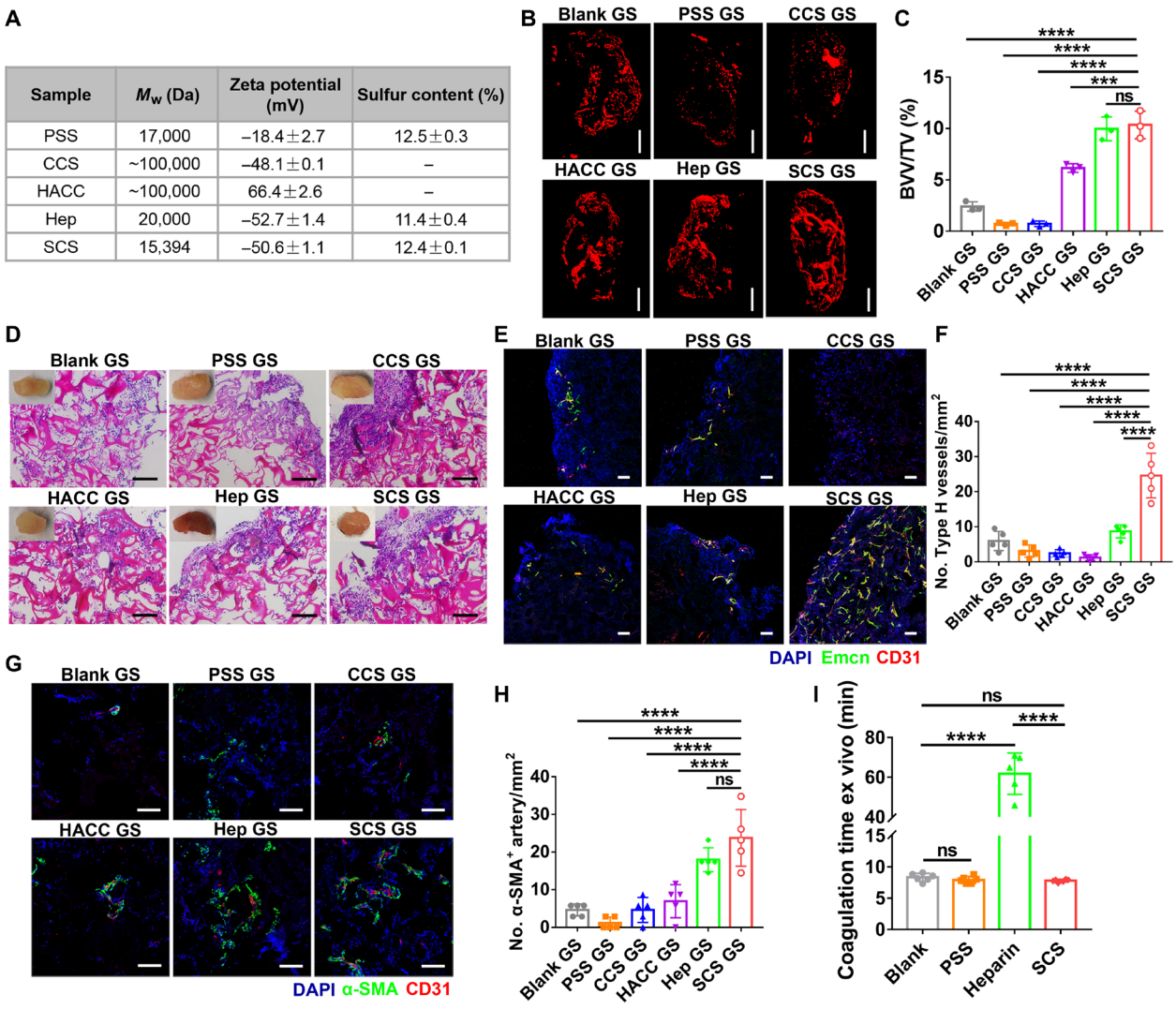


**Fig. 2. Angiogenic activity of various polymers.** (**A**) Characterization of the polymers by zeta potential analysis and elemental analysis. (**B** and **C**) Representative angiographic images (B) and quantification of relative blood vessel volume (BVV/TV) (C) in implants at day 7, respectively ($n = 3$). Scale bars, 1 mm. (**D**) H&E staining of implants at day 7 in mice ischemic hind limb. Scale bars, 100 μm. Insets are macroscopic views of the indicated implants. Photo credit: Y.Y., East China University of Science and Technology. (**E** to **H**) Representative immunostained images (E and G) with quantification of $CD31^{hi}Emcn^{hi}$ (Type H) endothelium (F) and α-$SMA^+$ arteries (H) in implants on day 7 after implantation in ischemic limb ($n = 5$). Scale bars, 100 μm. (**I**) Measurement of ex vivo anticoagulation; 2 μg of PSS, heparin, or SCS was added into 200 μl of blood plasma from rabbit at 37°C ($n = 6$). Data are means ± SD. ***$P < 0.05$ and ****$P < 0.001$; ns, not significant [(C), (F), and (H), one-way ANOVA compared to SCS GS with Dunnett's post hoc test; (I), one-way ANOVA compared to heparin with Dunnett's post hoc test].

in vitro in the presence of exogenous VEGF. The result indicated that SCS and Hep significantly up-regulated the VEGF-mediated phosphorylation of VEGFR2, while PSS inhibited the expression of phosphorylated VEGFR2 (fig. S4, L and M). Collectively, these results suggest that both SCS GS and Hep GS efficiently induce angiogenesis in ischemia, while PSS and positively or negatively charged chitosan have no effect on angiogenesis.

Ideal biomaterials for tissue regeneration should not be anticoagulant because the hematoma formed at the first stage of wound repair is beneficial for the recruitment of inflammatory cells, fibroblasts, and stem cells (*22*). Although the anticoagulant properties of natural sulfated polysaccharide heparin are well established, we observed that SCS did not have an anticoagulant ability (Fig. 2I). This observation suggests that SCS does not interfere with the coagulation cascade. Thus, we believe that SCS is an ideal bioactive material for regulating in situ angiogenesis.

SCS promotes angiogenesis by regulating VEGF secretion from Mφs

Next, to examine whether myeloid cells function to SCS-mediated angiogenesis, we first identified the presence of neutrophils ($CD45^+Ly6G^+CD11b^+$ cells) and Mφs ($CD45^+Ly6G^-CD11b^+F4/80^+$ cells) in SCS GS and Blank GS (Fig. 3, A and B). Flow cytometry data showed that neutrophil levels in both Blank GS and SCS GS rapidly decreased over time, whereas Mφs levels remained mostly constant. Nevertheless, no significant differences in neutrophils or Mφs recruitment to the implants were observed between SCS GS and Blank GS at days 7 and 14. As Mφs can be subsequently shifted to diverse functional phenotypes by local environmental cues, we therefore analyzed the phenotype of infiltrating Mφs in implants

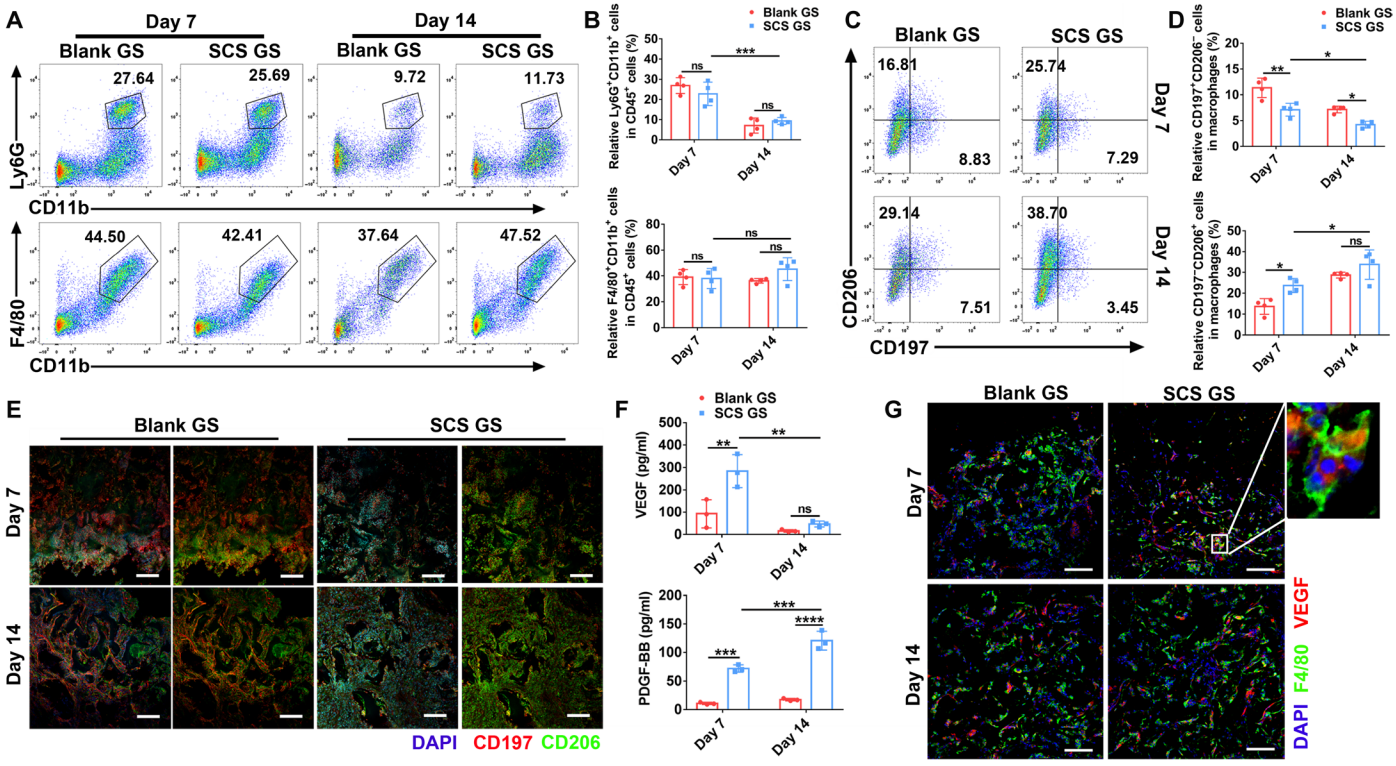


**Fig. 3. SCS increased the recruitment of M2 Mφs to the implants in ischemic limb.** (**A** and **B**) Representative flow cytometry plots (A) with quantification (B) of Ly6G$^+$CD11b$^+$ cells (neutrophils) and F4/80$^+$CD11b$^+$ cells (Mφs) from Blank GS and SCS GS on days 7 and 14 after implantation in ischemic limb ($n = 4$). (**C** and **D**) Representative flow cytometry plots (C) with quantification (D) of CD197$^+$CD206$^-$ Mφs (M1) and CD197$^-$CD206$^+$ Mφs (M2) polarization in Blank GS and SCS GS ($n = 4$). (**E**) Representative immunostainings of CD197 and CD206 in Blank GS and SCS GS on days 7 and 14 after implantation in ischemic limb. Scale bars, 200 μm. (**F**) VEGF and PDGF-BB concentrations by ELISA in Blank GS and SCS GS on days 7 and 14 after implantation ($n = 4$). (**G**) Representative immunostainings of VEGF secretion and F4/80$^+$ Mφs in Blank GS and SCS GS on days 7 and 14 after implantation in ischemic limb. Scale bars, 100 μm. Data are means ± SD. *$P < 0.05$, **$P < 0.01$, ***$P < 0.005$, and ****$P < 0.001$; ns, not significant (two-way ANOVA with Tukey's post hoc test).

after artery ligation. SCS GS recruited higher numbers of M2 Mφs (CD45$^+$Ly6G$^-$CD11b$^+$F4/80$^+$CD197$^-$CD206$^+$ cells) compared to Blank GS (Fig. 3, C and D), and a lower level of M1 Mφs (CD45$^+$Ly6G$^-$CD11b$^+$F4/80$^+$CD197$^+$CD206$^-$ cells) in SCS GS was observed compared to that in Blank GS. Immunostainings further confirmed that SCS GS was more conducive to the Mφs M1-to-M2 shift relative to Blank GS. M2 Mφs were spatially distributed around the implants, whereas M1 Mφs penetrated into the implants (Fig. 3E).

Next, to examine the potential molecular mechanism by which Mφs regulates angiogenesis, we collected fresh tissue fluid from the implants and detected the levels of two typical angiogenic growth factors by ELISA. The platelet-derived growth factor–BB (PDGF-BB) concentration in implants was significantly higher in SCS GS than in Blank GS, and the secretion level continually increased over time (Fig. 3F). VEGF concentration in SCS GS was also significantly higher than in Blank GS at day 7 and subsequently lowered by 83.4% in SCS GS at day 14 (Fig. 3F), consistent with the regeneration of Type H vessels and arteries. In addition, immunostainings demonstrated that most of the endogenous VEGF colabeled with F4/80$^+$ Mφs in implants (Fig. 3G). The area of F4/80$^+$ Mφs was not different between SCS GS and Blank GS, indicating that SCS had no effect on the recruitment of Mφs (fig. S5, A and B).

Consistent with the ELISA data, the percentage of VEGF-positive area in SCS GS slides was significantly higher than that in Blank GS on day 7 and showed a substantial reduction on day 14 (fig. S5, A and C). Acute injury and ischemia can lead to tissue hypoxia, which activates the pathway of hypoxia-inducible factor–1α (HIF-1α) and thus up-regulates the VEGF-mediated neoangiogenesis (*23*). Western blot analysis revealed that the early ischemic injury induced high expression of HIF-1α at day 7, and decreased HIF-1α protein levels were detected at day 14 (fig. S5, D and E).

Given that the hypoxia condition could significantly stimulate the VEGF secretion of Mφs to induce angiogenesis, we then examined the SCS-mediated angiogenesis in non-ischemia models. Laser Doppler imaging revealed that SCS GS improved the perfusion at the implanted site by days 3 and 7 in non-ischemia, and its level appeared to be higher than that in ischemia (fig. S6, A and B). Specially, we found that the number of Type H vessels and arterioles in non-ischemia was lower than that in ischemia (fig. S6, C to F). In addition, immunostainings revealed that non-ischemic condition reduced the infiltration of F4/80$^+$ Mφs into SCS GS compared to that in ischemia (fig. S6, G and H).

Mφ-lineage tartrate-resistant acid phosphatase–positive (TRAP$^+$) preosteoclasts have been reported to induce Type H vessel formation during bone modeling and remodeling via PDGF-BB secretion (*10*). To determine whether preosteoclasts participate in the regulation of angiogenesis in this system, we conducted TRAP staining to identify Mφs and preosteoclasts. The results showed that almost no

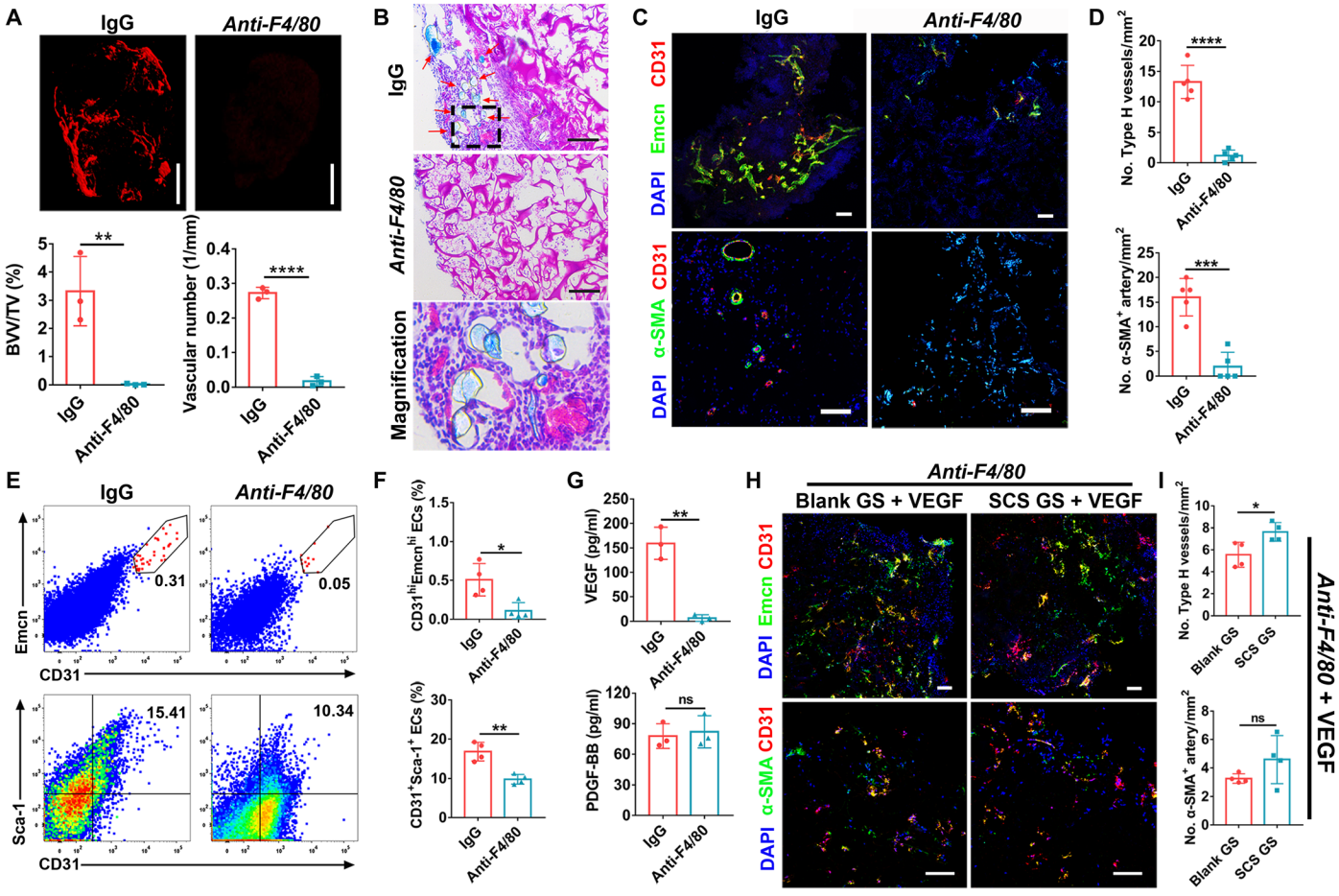


**Fig. 4. Mφs depletion impairs the VEGF-mediated angiogenesis in ischemia.** (**A**) Representative angiographic images (top) and quantification (bottom) of relative blood vessel volume (BVV/TV) and vascular number of SCS GS at day 7 ($n = 3$). Scale bars, 1 mm. (**B**) H&E staining of SCS GS in Mφs depletion treatment. Red arrows indicate the Microfil-perfused blood vessels. Scale bars, 100 μm. (**C** and **D**) Representative immunostainings (C) with quantification (D) of CD31$^{hi}$Emcn$^{hi}$ (Type H) endothelium and α-SMA$^{+}$ arteries in SCS GS 7 days after depletion treatment ($n = 5$). Scale bars, 100 μm. (**E** and **F**) Representative flow cytometry plots (E) with quantification (F) of CD31$^{hi}$Emcn$^{hi}$ and CD31$^{+}$Sca-1$^{+}$ endothelial cells from SCS GS on day 7 in Mφs-depleted mice ($n = 4$). (**G**) VEGF and PDGF-BB concentrations by ELISA in SCS GS on day 7 in Mφs-depleted mice ($n = 3$). (**H** and **I**) Representative immunostainings (H) with quantification (I) of the implants loaded with 100 ng of exogenous VEGF on day 7 after implantation in Mφs-depleted mice ($n = 4$). Scale bars, 100 μm. Data are means ± SD. *$P < 0.05$, **$P < 0.01$, ***$P < 0.005$, and ****$P < 0.001$; ns, not significant (unpaired two-tailed Student's $t$ test).

TRAP$^{+}$ cells were observed in the implants on day 7, and TRAP$^{+}$ cells were observed rarely on day 14 (fig. S5, F and G). As the time point of TRAP$^{+}$ cell recruitment was not consistent with the formation of Type H vessels or arteries, we concluded that TRAP$^{+}$ cells rarely participate directly in the recruitment of endothelial cells or angiogenesis in this system. Together, these observations suggest that SCS could efficiently promote the phenotype switch of M1-to-M2 Mφs and stimulate the endogenous VEGF secretion to induce angiogenesis in ischemia.

To further examine the role of Mφs in SCS-induced angiogenesis in ischemia, we continuously administered rat immunoglobulin G2b (IgG2b) anti-mouse F4/80 antibody every day for 9 days to deplete the circulating Mφs in ischemic mice and assessed the simultaneous angiogenesis. Simultaneous injection of rat IgG2b antibody was used as a control. SRμCT analysis revealed that depletion of circulating Mφs was detrimental to angiogenesis in ischemia, and the relative blood vessel volume and vascular number were significantly lower than the IgG (Fig. 4A). Histology analysis showed that SCS GS implanted into anti-F4/80–treated mice displayed less invasion of inflammatory cells, and almost no fibrous connective tissue or vascular-like tissue was found to grow into the implants (Fig. 4B). Coimmunostainings of CD31 and Emcn demonstrated that the number of Type H vessels in anti-F4/80–treated mice significantly decreased relative to that in IgG-treated mice, and no α-SMA$^{+}$ arteries or vascular lumens were detected in anti-F4/80–treated mice (Fig. 4, C and D). Flow cytometry analysis also confirmed that Mφs depletion significantly inhibited the formation of CD31$^{hi}$Emcn$^{hi}$ endothelium (Fig. 4, E and F).

In addition, Mφs depletion significantly decreased VEGF concentration in SCS GS but had no effect on PDGF-BB concentration (Fig. 4G). To validate that Mφs depletion inhibited angiogenesis by down-regulating VEGF secretion, we treated the implants with 100 ng of exogenous VEGF. As expected, both Blank GS and SCS GS rescued the formation of Type H vessels in anti-F4/80–treated mice after loading exogenous VEGF (Fig. 4, H and I). However, the

introduction of exogenous VEGF had no effect on arterial rescue (Fig. 4, H and I). These results reveal that VEGF secreted by Mφs predominantly stimulates Type H vessels in ischemia.

### SCS promotes Mφs-mediated angiogenesis via VEGF-induced VEGFR2 signaling pathway

Mouse peritoneal Mφs that developed from bone marrow–derived monocytes were widely used as primary cells to investigate the physiological and pathophysiological processes of inflammatory diseases. Thus, we chose mouse peritoneal Mφs as a cell model to examine the mechanism of how SCS regulated the Mφs-mediated angiogenesis. The isolated mouse peritoneal Mφs were of high purity (fig. S7A), and we found that SCS had no effect on the cell viability of Mφs at a series of concentrations (fig. S7C). We subsequently examined the effects of different concentrations of SCS on the sprouting of rat aortic rings under mouse peritoneal Mφs coculture conditions and screened the optimal concentration of SCS at 800 ng/ml in vitro (fig. S7, D and E). We found that SCS cocultured with Mφs significantly promoted the formation of tip cells in the sprouts of aortic rings with high expression of VEGFR2 (fig. S8A).

To further clarify the mechanism of Mφs in promoting angiogenesis, we harvested the conditioned medium from Mφs (Mφs CM) or Mφs stimulated by SCS (SCS/Mφs CM) to culture with HUVECs. SCS/Mφs CM exhibited an enhanced ability to induce migration of endothelial cells and formation of capillary tubes compared to Blank and Mφs CM (fig. S8, B to E). In addition, we found that the cumulative tube length of sprouted endothelial cells with treatment of 3-day SCS/Mφs CM was more than that of 7-day SCS/Mφs. Cell number of mouse peritoneal Mφs decreased with incubation time, consistent with a terminally differentiated cell (fig. S7B). This is why the 7-day Mφs CM decreased the angiogenic activity of HUVECs compared to the stimulation of 3-day Mφs CM. Consistent with the angiogenic behavior in vitro, VEGF secreted by Mφs was significantly elevated after stimulation by SCS for 3 days and further decreased at day 7 (Fig. 5A). In contrast, SCS significantly promoted the expression of endogenous PDGF-BB at both days 3 and 7, and the concentration did not change with the culture time (Fig. 5A).

We next investigated the trafficking of VEGFR2, a major receptor transducing signaling in endothelial cells, and asked whether SCS stimulated Mφs CM–induced VEGFR2 phosphorylation in HUVECs. First, we incubated endothelial cells and macrophages with fluorescein isothiocyanate (FITC)–labeled SCS and analyzed the fluorescence intensity of cells to examine whether SCS could be internalized by cells. The results indicated that a stronger binding interaction of SCS was observed in Mφs relative to that in endothelial cells, and incubation at 4°C had no impact on the strength of the fluorescent signal relative to incubation at 37°C (fig. S8, F and G). As an active internalization mediated by endocytosis is energy dependent and would have been strongly reduced by incubation at 4°C (*24*), this result suggests that SCS is not internalized by cells. Further, immunostainings revealed that abundant localized puncta of VEGFR2 on HUVECs were found after 3-day SCS/Mφs CM treatment (Fig. 5B). Almost no VEGFR2 internalization was detected in Blank or 7-day Mφs CM treatment. Moreover, 3-day SCS/Mφs CM activated transduction of the VEGF signaling cascade in HUVECs, as revealed by the increased phosphorylation of VEGFR2 and its downstream mediators focal adhesion kinase (FAK) and Akt (Fig. 5, C and D, and fig. S8, J to L), while SCS itself could not induce the phosphorylation of VEGFR2, which meant that SCS alone could not enhance the angiogenic activity of endothelial cells (fig. S8, H and I).

To further verify the proangiogenic capacity of SCS/Mφs CM functions in a VEGF-VEGFR2 signaling pathway, we used inhibitors to antagonize VEGF or VEGFR2 to investigate its effect on the regulation of SCS/Mφs CM in promoting angiogenesis. SCS/Mφs CM with VEGF neutralizing antibody (NAb) or VEGFR2 inhibitor significantly reduced its VEGFR2 phosphorylation and the length of tube formation (Fig. 5, E to H), which again suggested that SCS/Mφs CM exerted its angiogenic effect via VEGF signaling, especially involving VEGFR2. In addition, the expression of *VE-cadherin*, *CD31*, and *VEGF* in HUVECs exposed to the SCS/Mφs CM was also attenuated by VEGF NAb or VEGFR2 inhibitor relative to Blank (Fig. 5I). Thus, these results suggest that SCS positively regulates VEGF secretion in Mφs and mediates VEGF-induced angiogenesis through VEGFR2 signal transduction.

### SCS directs the immunomodulation of Mφs

Although the above results indicate that SCS can significantly promote Mφ-mediated angiogenesis, the effect of introduced SCS on immunomodulation of Mφs was not clear. Thus, we first investigated the gene expression of Mφs after stimulation for 3 and 7 days with SCS, including canonical proinflammatory genes (*Il-1b*, *Tnf-a*, and *Il-6*), anti-inflammatory genes (*Il-1ra*, *Il-4*, and *Il-10*), and Mφs phenotype markers (*Cd163*, *Cd197*, and *Cd206*). Gene expression analysis showed that SCS significantly down-regulated the proinflammatory cytokines of *Il-1b* and *Tnf-a* and the surface marker *Cd197*. In contrast, genes associated with anti-inflammatory cytokines (*Il-4* and *Il-10*) and surface markers (*Cd163* and *Cd206*) were significantly up-regulated after 3 days with SCS treatment (fig. S9). Flow cytometry analysis showed that SCS could efficiently stimulate the M1-to-M2 polarization of Mφs (fig. S10, A and B). Immunostainings showed more positive CD206 puncta on the Mφs after treatment with SCS. In addition, the morphology of Mφs appeared as a long strip shape with abundant pseudopodia after treatment with SCS, which is a canonical morphology of M2 Mφs (fig. S10C).

Canonical signal transducers and activators of transcription (Stat) signaling pathways are known to mediate Mφ polarization (*25*); we therefore examined the mechanism of how SCS regulated Mφ polarization. ELISA analysis revealed that SCS significantly improved the secretion of endogenous interleukin-4 (IL-4) relative to that of Blank (fig. S10D). In addition, Western blot analysis showed that SCS could significantly activate the phosphorylation of Stat6 in Mφs by 20 min after incubation, whereas no significant difference in phosphorylation of Stat3 was observed between SCS and Blank (fig. S10, E and F). The results indicate that the phosphorylation of Stat6 signaling mediates SCS-induced M2 Mφ polarization.

Next, to investigate the effect of SCS on inflammatory and anti-inflammatory cytokine secretions of Mφs, a mouse cytokine array assay was performed. Cytokine levels of CM treated for 7 days with SCS showed widespread down-regulation of numerous inflammatory cytokine [most notably RANTES, SDF-1α, and TNF-α (tumor necrosis factor–α)] and up-regulation of anti-inflammatory IL-1rα relative to Mφs CM (fig. S10, G and H), which coincided with the transition of M1-to-M2 Mφs polarization. In addition, we found that the level of MCP-1 (monocyte chemoattractant protein-1)

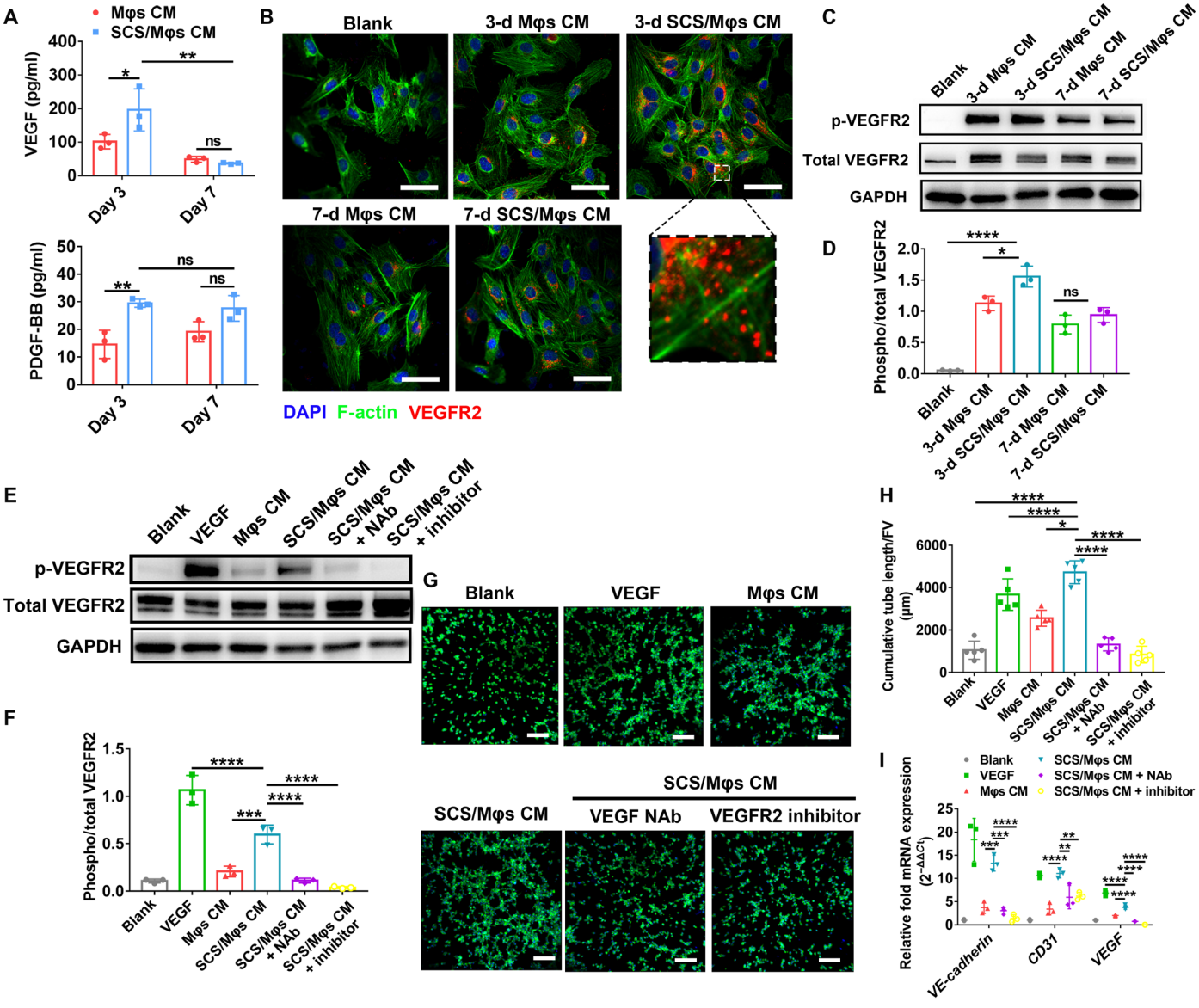


**Fig. 5. SCS/Mφ CM induces angiogenic function via VEGF-VEGFR2 signaling pathway.** (**A**) ELISA analysis of the concentration of VEGF and PDGF-BB in SCS/Mφs conditioned media. (**B**) Immunofluorescence of VEGFR2 on HUVECs after treatment with indicated CM stimulation for 10 min. Scale bars, 50 μm. (**C** to **F**) Western blot analysis (C and E) and the relative level (D and F) of phosphorylated VEGFR2 after treating with the indicated CM for 10 min. (**G** and **H**) Representative tubular network formation images (G) of HUVECs and quantitative analysis of cumulative tube length (H) using 3-day SCS/Mφs CM after treating with VEGF neutralizing antibody (NAb) or VEGFR2 inhibitor ($n = 6$). Scale bars, 200 μm. (**I**) Quantitative real-time polymerase chain reaction (qRT-PCR) analysis of *VE-cadherin*, *CD31*, and *VEGF* with the treatment of 3-day SCS/Mφs CM with VEGF NAb or VEGFR2 inhibitor. Data are means ± SD. *$P < 0.05$, **$P < 0.01$, ***$P < 0.005$, and ****$P < 0.001$; ns, not significant [(A), two-way ANOVA with Tukey's post hoc test; (D), one-way ANOVA with Tukey's post hoc test; (F), (H), and (I), one-way ANOVA compared to SCS/Mφs CM with Dunnett's post hoc test].

in Mφs CM did not show a significant difference compared with the SCS/Mφs CM, which is the main chemokine for the recruitment of Mφs. To further investigate the inflammatory response of SCS GS after ischemic injury, we examined the cytokine levels in vivo using an ELISA kit. After implantation for 7 and 14 days, we collected the tissue fluid by immersing Blank GS and SCS GS pieces into 500 μl of cold phosphate-buffered saline (PBS) and quantified their levels of cytokines [IL-1β, TNF-α, IL-4, IL-6, IL-10, and TGF-β1 (transforming growth factor–β1)]. We found that SCS GS significantly decreased the concentration of TNF-α at 7 days after implantation (fig. S11).

## SCS rescues the regeneration of CD31$^{hi}$Emcn$^{hi}$ vessels in models of Mφs inhibition

Chronic excess Mφs aggregation always results in chronic diseases, including atherosclerosis, asthma, inflammatory bowel disease, rheumatoid arthritis, and fibrosis (*26*). To counteract the tissue-damaging potential of the inflammatory Mφ response, Mφs undergo apoptosis, which dampens the proinflammatory response while facilitating wound healing (*27*). However, drugs that indiscriminately eliminate Mφs in inflammatory-related diseases may also inhibit the secretion of therapeutic growth factors and slow the healing of wound. As SCS significantly stimulated the in situ VEGF

secretion from Mφs and our previous study verified that SCS could efficiently promote angiogenesis with the aid of extremely low doses of VEGF (*19*), we hypothesized that SCS may have therapeutic effects to promote angiogenesis in low Mφs response. To examine this, we first administered anti-F4/80 antibody every day for the first 9 days via orbital injection in hind limb ischemic mice to totally deplete the Mφs and then injected it every other day to ensure a small-number recovery of Mφs in peripheral blood. Flow cytometry analysis confirmed that Mφs were totally depleted at day 7 and a small amount of Mφs were recovered at day 14 (Fig. 6A). After 16 days of treatment, histological analysis showed a significantly increased presence of perfused vessels with a distinct invasion of fibroid

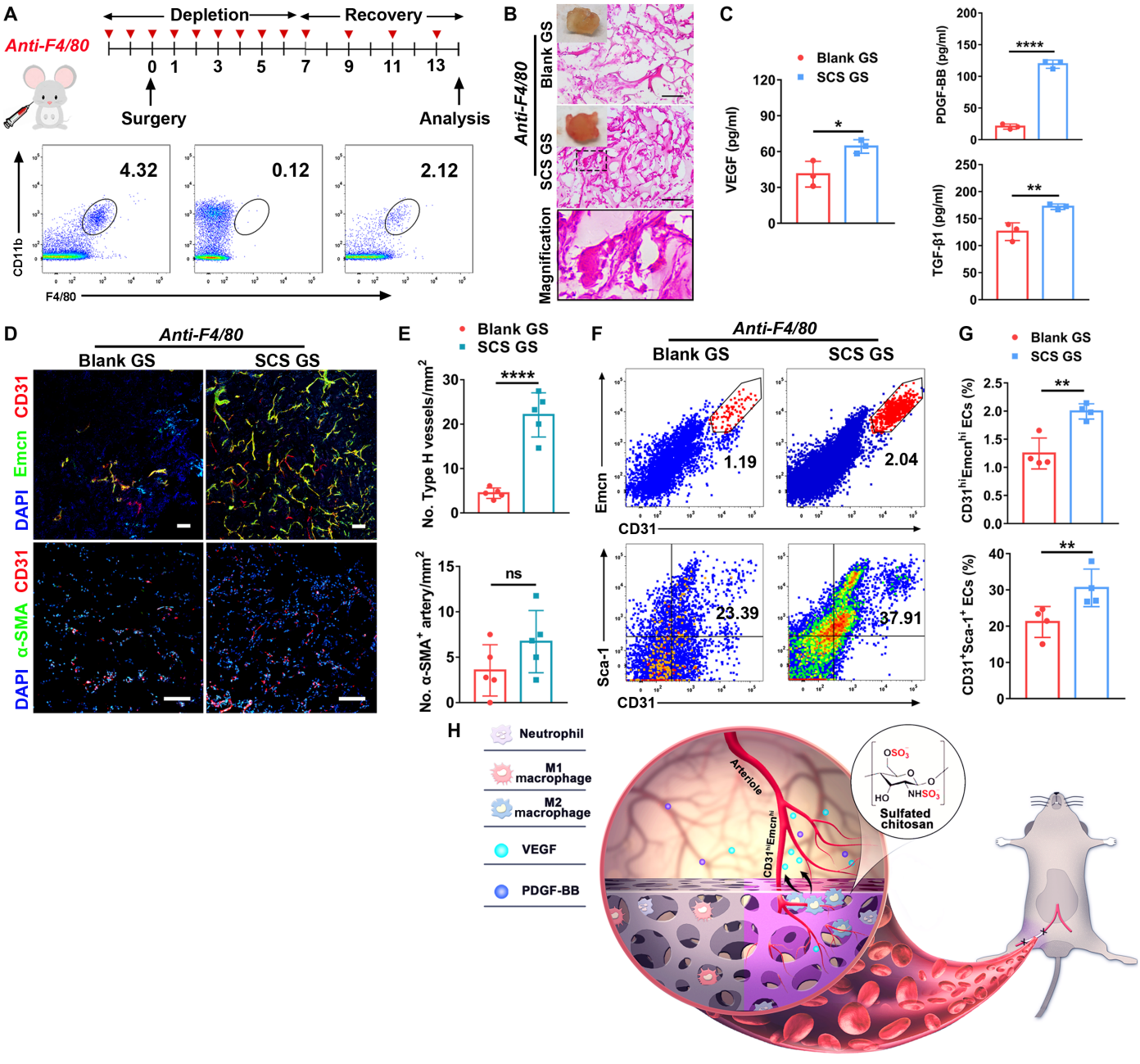


**Fig. 6. SCS rescues angiogenesis in Mφ-inhibited mice.** (**A**) Schematic with Mφs depletion and reduction strategies. The flow cytometry plots represent the Mφs proportion in peripheral blood 2 days before operation and 7 and 14 days after operation, from left to right, respectively. (**B**) H&E analysis of implants on day 14 in Mφ-inhibited mice. Scale bars, 100 μm. Photo credit: Y.Y., East China University of Science and Technology. (**C**) VEGF, PDGF-BB, and TGF-β1 concentrations by ELISA in retrieved implants on day 14 ($n = 3$). (**D** and **E**) Representative immunostainings (D) with quantification (E) of $CD31^{hi}Emcn^{hi}$ (Type H) endothelium and $\alpha$-$SMA^{+}$ arteries in Blank GS and SCS GS on day 14 in Mφ-inhibited mice ($n = 5$). Scale bars, 100 μm. (**F** and **G**) Representative flow cytometry plots (F) with quantification (G) of $CD31^{hi}Emcn^{hi}$ and $CD31^{+}Sca\text{-}1^{+}$ endothelial cells from Blank GS and SCS GS on day 14 in Mφ-inhibited mice ($n = 4$). (**H**) Illustration of SCS to induce therapeutic angiogenesis. In mice ischemic hind limb model, SCS promotes the polarization of M1-to-M2 Mφs with stimulating secretion of endogenous VEGF to induce arterioles and $CD31^{hi}Emcn^{hi}$ vessels. Data are means ± SD. $^{*}P < 0.05$, $^{**}P < 0.01$, and $^{****}P < 0.001$; ns, not significant (unpaired two-tailed Student's *t* test).

tissue in SCS GS after a small recovery of Mφs (Fig. 6B). The VEGF, PDGF-BB, and TGF-β1 concentrations were significantly higher in SCS GS implants than in Blank GS (Fig. 6C), which indicated that SCS is more conducive to in situ capture of endogenic angiocrine.

To further confirm the function of SCS in vasculature reconstruction, we examined the phenotype of vessels generated in the implants. Immunostainings and flow cytometry analysis showed that the formation of $CD31^{hi}Emcn^{hi}$ endothelium in implants was significantly augmented by SCS GS relative to the Blank GS after the recovery of Mφs (Fig. 6, D to G). Particularly, although flow cytometry data revealed that abundant arterial endothelial cells grew into the implants after the recovery of Mφs (Fig. 6, F and G), $\alpha\text{-SMA}^{+}$ cell–encapsulated arteries were still difficult to observe in both Blank GS and SCS GS (Fig. 6, D and E). This result indicates that the destruction of Mφs is irreversible in terms of the reconstruction of the artery. Together, these results show that SCS significantly rescues the regeneration of Type H vessels once the Mφs are inhibited and may have clinical utility to treat angiogenesis in some low immune response diseases.

## DISCUSSION

Adequate vascular growth and rapid host integration with nutrient infusion are essential for successful translation of implants in tissue engineering. In our previous work, we reported that SCS significantly promoted angiogenesis by up-regulating the VEGF-VEGFR2 interaction (*19*). Although angiogenesis is mediated mainly by endothelial cells, it is likely that myeloid cells affected by SCS are also involved in inducing angiogenesis. In addition to inducing sufficient blood vessels to the injury site, the high heterogeneity of endothelial cells with specialized functional properties in local microenvironments is also of concern (*28*). However, how implant-associated Mφs affect the local angiogenic milieu remains poorly understood. This study showed that SCS GS provoked Mφs to secrete VEGF and promote angiogenesis and vascular perfusion in ischemia (Fig. 6H). SCS GS induced the formation of mature and highly developed arteries within the ischemic cavity accompanied with the ingrowth of $CD31^{hi}Emcn^{hi}$ vessels, a specific vessel subtype with distinct morphological and molecular properties that only exists where bone is present (*20*). Depletion of Mφs effectively decreases the concentration of VEGF and inhibits the formation of arteries and $CD31^{hi}Emcn^{hi}$ vessels. In particular, SCS significantly promoted the regeneration of $CD31^{hi}Emcn^{hi}$ vessels after Mφs were inhibited. This angiogenic biomaterial with no exogenous growth factors represents a potential therapeutic strategy for ischemia, especially in some inflammatory diseases.

Accumulating evidence indicates that Mφs can comprise two distinct subpopulations: a canonical proinflammatory phenotype (M1) and an alternative pro-healing phenotype (M2) (*29*). Mφs secrete growth factors and inflammatory cytokines that support angiogenesis by promoting endothelial cell survival, sprouting, and proliferation. However, little is known about the mechanism that regulates angiogenesis via implant-activated Mφs in vivo. Here, we showed that the implanted SCS GS significantly promoted the phenotype shift of Mφs toward the M2 state with a high local concentration of VEGF, which is consistent with previous reports that $CD206^{+}$ Mφs are a rich source of VEGF production (*30*). As canonical Stat signaling pathways are activated by IL-4 or IL-10 to skew toward the M2 phenotype via Stat6 or Stat3 pathway (*25*), SCS skewed Mφs function toward M2 phenotype via IL-4–mediated Stat6 signaling pathway rather than IL-10–mediated Stat3. Depleting Mφs significantly inhibited angiogenesis in SCS GS, while introducing exogenous VEGF rescued the formation of $CD31^{hi}Emcn^{hi}$ vessels in Mφ-depleted mice. This distinct vascular formation is supported by the differential VEGFR2 phosphorylation signaling of VEGF from Mφs. However, we found that depletion of Mφs is irreversible in terms of arteriogenesis, and increasing evidence indicates that arteriogenesis is closely related to Mφs maturation and polarization (*31*). Impaired Mφs will lead to reduced release of arteriogenic factors and, in turn, inhibit the recruitment of smooth muscle cells.

Beyond Mφs recruitment and polarization, the HIF-1α pathway also regulates the secretion of Mφ-associated VEGF and angiogenesis (*23*). Although a large number of M2 Mφs remained on day 14, we found that the expression of HIF-1α and VEGF progressively declined, which led to a rapid decrease in the number of $CD31^{hi}Emcn^{hi}$ vessels and arteries in implants. Although our study focused on the role of Mφs in biomaterial vascularization, the implants also induced early invasion of neutrophils. Neutrophils present mainly acted as cellular chaperones for vascular anastomosis (*6*) and contributed to angiogenesis by secreting matrix metalloproteinase–9 (MMP-9) to release angiogenic growth factors bound to the extracellular matrix (*32*), which was expected in light of their role in inducing angiogenesis in this study.

Implant-associated Mφs are required to induce neovessels, whereas an excessive release of cytokines will aggravate the foreign body reaction (*12*). Here, we showed that SCS lowered the expression of canonical proinflammatory genes and cytokines of Mφs and decreased the concentration of TNF-α in ischemia. Mounting evidence indicates that sulfated polymers have many anti-inflammatory effects linked to their ability to inhibit leukocyte adhesion by blocking L-selectin binding (*33*) and to stabilize chemokine and growth factors (*34*). We hypothesize that SCS could efficiently sequester inflammatory chemokines in the early stages of acute inflammation, thereby preventing further M1 Mφ polarization.

Polysaccharides with affinity for growth factors are mainly mediated through electrostatic interaction, heparin-binding domain, and spatial conformation. Engineered substitutes with sulfated groups have been established that could efficiently bind growth factors. Here, we showed that SCS and heparin significantly promoted angiogenesis in ischemia and elevated the expression of angiogenic-related genes. As typical chitosan derivatives, CCS and HACC could not induce VEGF-mediated angiogenesis. This is mainly because carboxylates are known to form weaker salt bridges with the side chains of lysine and arginine in the heparin-binding domains of VEGF relative to sulfates (*35*), and the positively charged polysaccharide is considered to be unbound to protein. Notably, PSS significantly inhibited the formation of blood vessels, although the polymer could stabilize FGF-2 (fibroblast growth factor 2) and VEGF via the heparin-binding domains (*36*). In addition, the anticoagulant properties of heparin and analogs are well established, and the 3-O-sulfated group and carboxyl groups within heparin are essential for binding to antithrombin III (*37*, *38*). SCS does not exhibit anticoagulant activity because of its selective sulfonation modification and noninvolvement of carboxyl groups. In addition, a previous study suggested that the anticoagulant activity was also associated with the concentration of sulfated chitosan derivatives, and the anticoagulation improved with the increase of the concentration

(*38*). The high purity of SCS ensured its biological activity at low dosage and efficiently reduced the risk of anticoagulation. Together, these results more broadly suggest that both sulfated group and carbohydrate structure in SCS are essential for inducing angiogenesis in ischemia.

In summary, our finding showed that SCS GS induced angiogenesis and rapidly achieved blood flow penetration in ischemia without the aid of exogenous angiogenic-related growth factors. Unexpectedly, SCS did not have heparin-like anticoagulant activity and exhibited an anti-inflammatory property. Although information on the effect of molecular weight and polysaccharide sequence arrangement on angiogenesis was not experimentally demonstrated in this study, it was clear that SCS can induce Type H vessels and arteries by directing immune response of Mφs with VEGF secretion. We believe that these findings provide insight into the Mφ-mediated angiogenesis induced by immunomodulation of SCS and may allow the development of tractable biomaterial-based therapeutic angiogenesis treating the ischemic defects and diseases.

## MATERIALS AND METHODS

### Materials

Chitosan [molecular weight ($M_w$): ~$30 \times 10^4$ Da, 92% deacetylated] was obtained from Shenzhen Zhongfayuan Biological Technology Co. Ltd. (Shenzhen, China). PSS ($M_w$: $1.7 \times 10^4$ Da) was purchased from Sigma-Aldrich (St. Louis, MO, USA). CCS ($M_w$: ~$1.0 \times 10^5$ Da) and HACC ($M_w$: ~$1.0 \times 10^5$ Da) were purchased from Yuanye Biotech. Co. Ltd. (Shanghai, China). Growth factor–reduced Matrigel Matrix and rat tail collagen type I were obtained from Corning Inc. (Corning, NY, USA). TRIzol reagent, PrimeScript RT reagent kit, and SYBR Premix Ex Taq were purchased from Takara Biotechnology Co. Ltd. (Dalian, China). Gelatin sponge (GS) was purchased from Xiang'en Medical Technology Development Co. Ltd. (Jiangxi, China). SCS was synthesized as previously described (*39*). A FluoroTag™ FITC Conjugation kit (FITC1, Sigma-Aldrich) was used to label SCS with FITC according to the manufacturer's instructions. All cell culture–related reagents were available from Gibco (Grand Island, NY, USA).

### Preparation of polysaccharide-coated gelatin sponge

The gelatin sponges were cut into pieces (0.8 cm × 0.8 cm × 0.8 cm) under sterile condition. The polysaccharides were dissolved in PBS to obtain a 0.125% solution. Subsequently, 40 μl of SCS, PSS, CCS, HACC, and Hep was dropped onto the gelatin sponges in sterile condition and stayed for a while to be totally absorbed. The equal volume of PBS was added onto the sponge as blank group. The polysaccharide-coated gelatin sponges were lyophilized and stored at −20°C. The release kinetics of SCS from gelatin sponge was detected as previously reported (*40*).

### Mouse ischemic hind limb model

Male C57BL/6 mice (6 weeks old, Slac Laboratory) were anesthetized with 2% isoflurane at a flow rate of 0.4 liter/min. Following hair removal and skin incision, the right femoral neurovascular pedicle was visualized under a stereomicroscope (RWD), and the femoral nerve and vein were carefully separated from the femoral artery. The femoral artery was surgically ligated with two double knots distal to the origin of the deep femoral branch and transected with scissors. GS containing 50 μg of SCS or vehicle was implanted into muscle below the site of the segmented artery, and the surgical site was sutured. Laser Doppler imaging (Moor Instruments) was performed to investigate the perfusion of new vessels at 6 hours and on days 3, 7, 14, and 28 after surgery. Results are expressed as fold increase/decrease of perfusion units of implant area (region of interest) with respect to the contralateral region. Animals were randomly assigned to groups. All surgical procedures were approved by the Institutional Animal Care and Use Committee of East China Normal University.

### Angiography

SRμCT was used to image the new vessels in ischemia. Briefly, after opening the thoracic cavity of mice, a needle was inserted into the left ventricle and the vasculature was flushed with heparinized saline [0.9% saline containing heparin sodium (100 U/ml)]. Then, 5 ml of Microfil (MV-120, Flow Tech Inc.) was injected into the vasculature. The heart was ligated, and mice were stored at 4°C overnight. The retrieved implants were fixed with 4% paraformaldehyde and imaged by SRμCT, performed at the BL13W beamline of the Shanghai Synchrotron Radiation Facility (Shanghai, China) using a monochromatic beam with energy of 16 keV and a sample-to-detector distance of 0.8 m. In the current study, a 2048 × 2048 sCMOS detector (Flash 4.0, Hamamatsu City, Japan) with the pixel size set to 9 μm was used to record tomographies. Brucker software was used to visualize the 3D structure from slice images. Relative vascular volume and vascular number were measured.

### Histology and immunofluorescence

For histological analysis, retrieved implants were fixed in 4% neutral paraformaldehyde buffer for 48 hours, dehydrated, embedded, and sectioned at 7-μm thickness. Sections were stained with hematoxylin and eosin (H&E), and the neovascularization and tissue structure were microscopically examined. TRAP staining was finalized with a staining kit according to the manufacturer's instructions (Sigma-Aldrich).

For immunofluorescence, fresh samples were immediately fixed in ice-cold 4% paraformaldehyde solution for 4 hours at 4°C. After immersing into 20% sucrose and 2% polyvinylpyrrolidone overnight, all samples were embedded in OCT compound (Leica) and cut into sections. Immunofluorescence staining and analysis were performed as described previously (*41*). Briefly, after treatment with 0.3% Triton X-100 for 20 min, sections were blocked with 5% goat serum at room temperature for 1 hour and incubated overnight at 4°C with the antibodies CD31, Emcn, α-SMA, Ki67, F4/80, VEGF, CD197, and CD206. Primary antibodies were then visualized with species-appropriate secondary antibodies. The sections were mounted by ProLong Gold Antifade reagent with DAPI (4′,6-diamidino-2-phenylindole) (Cell Signaling Technology). A Nikon confocal microscope was used to image samples.

### Flow cytometry

Flow cytometry was used to assess cell recruitment and phenotype in the angiogenic implants in vivo. Briefly, samples were dissected from euthanized mice after removing the surrounding muscle. To obtain a single-cell suspension of endothelial cells, the retrieved implants were enzymatically digested with collagenase type I (3 mg/ml) (Gibco) and neutral protease (4 mg/ml) (Roche) for 15 min at 37°C. The resulting cell suspension was filtered (40 μm) and washed using a staining buffer. Murine cells were blocked with CD16/CD32

monoclonal antibody (eBioscience) for 30 min at 4°C. The immune cells and endothelial cells were assessed using two antibody groups. Immune cells were stained with allophycocyanin (APC)/Cy7–conjugated 7-amino-actinomycin D (7-AAD), phycoerythrin (PE)–conjugated CD45, peridinin chlorophyll protein (PerCP)/Cy5.5–conjugated Ly6G, Alexa Fluor 700–conjugated F4/80, BV450-conjugated CD11b, APC-conjugated CD197, and FITC-conjugated CD206 for 45 min at 4°C. Endothelial cells were first stained with rat anti-mouse Emcn antibody for 45 min at 4°C. After washing, cells were further incubated with APC/Cy7-conjugated 7-AAD, PE-conjugated CD45/Ter119, PE/Cy7-conjugated Sca-1, BV421-conjugated CD31, and Alexa Fluor 488–conjugated goat anti-rat IgG for 45 min at 4°C. The cell suspension was then assessed on an LSRFortessa$^{TM}$ X-20 flow cytometer system (BD Biosciences) and analyzed using FlowJo software (Tree Star). The strategy to analyze endothelial cells and inflammatory cells is diagrammed in fig. S12.

### Endothelial cell sorting

To obtain a single-cell suspension of endothelial cells, the retrieved implants were enzymatically digested with collagenase type I (3 mg/ml) (Gibco) and neutral protease (4 mg/ml) (Roche) for 15 min at 37°C. The resulting cell suspension was filtered (40 μm) and washed using sterile $Ca^{2+}$-and $Mg^{2+}$-free HBSS (Hanks' balanced salt solution). Leukocytes in the cell suspension were first depleted using mouse CD45 MicroBeads (Miltenyi Biotec) via negative selection and then sorted using CD31 antibody and anti-rat IgG MicroBeads (Miltenyi Biotec). The number of sorted endothelial cells was determined using the Countess II FL Automated Cell Counter (Invitrogen). Total RNAs were extracted from the sorted endothelial cells with TRIzol reagent, followed by a reverse transcription step with PrimeScript RT reagent kit according to the manufacturer's instructions. The reverse-transcribed complementary DNA (cDNA) was stored at −80°C until the quantitative real-time polymerase chain reaction (qRT-PCR) assay.

### Anticoagulation assay

Fresh rabbit blood was collected into a BD Vacutainer containing sodium citrate. The sodium citrate keeps the blood from clotting for 2 hours at 37°C. A total of 200 μl of blood was first mixed with 20 μl of 0.2 M $CaCl_2$ to neutralize the sodium citrate, and 20 μl of sulfated polymer (100 μg/ml, dissolved in PBS) was subsequently added into the blood. An equal volume of PBS was added to the Blank. The mixed solution was immediately placed at 37°C until complete coagulation, and the time of complete coagulation was recorded.

### HPLC analysis of SCS degradation

At days 3, 7, and 14 after SCS GS was implanted into the hind limb ischemia, mice were sacrificed and the retrieved implants were stored at −20°C. SCS GS was first homogenized in trichloroacetic acid (10%, v/v, in deionized water) and centrifuged at 12,000*g* for 10 min at 4°C to remove the precipitated proteins. The resulting supernatants were resuspended in acetone to remove the trichloroacetic acid and centrifuged at 12,000*g* for 10 min at 4°C. The SCS precipitation was redissolved in deionized water and analyzed by HPLC. The reversed-phase HPLC analysis used the combination of water (eluent A) and acetonitrile (eluent B) as the mobile phase with the gradient as follows: 0 to 9 min, 50 to 70% B; 9 to 10 min, 70% B. Sulfated chitosan and SCOS were used as standard samples.

### Mφs depletion

To completely deplete the Mφs, a rat IgG2b anti-mouse F4/80 (CI: A3-1, Bio X Cell) antibody was administered retro-orbitally at 400 μg per mouse 2 days before operation and then every day at 200 μg per mouse for 7 days. To investigate the effect of partially inhibited Mφs on angiogenesis, the antibody was sequentially injected at 200 μg per mouse every other day for another 7 days to ensure a low number recovery of Mφs. This process was mainly to investigate the revascularization of SCS in low-volume Mφs. InVivoMAb rat IgG2b (200 μg per mouse) served as a control. Mφs depletion was confirmed in peripheral blood by flow cytometry.

### Cell isolation and culture

After euthanization, we collected mouse peritoneal Mφs from 8-week-old male C57BL/6 mice. The isolated Mφs were allowed to recover and adhere in Dulbecco's minimum essential medium (DMEM) with 10% fetal bovine serum (FBS) and 1% penicillin/streptomycin for 4 hours. Thereafter, the nonadherent cells were removed by rinsing several times with PBS, and fresh growth medium was added. Purity of the cell population was identified by positive F4/80 and CD11b through flow cytometry (BD Accuri C6) after overnight incubation. Cell viability of Mφs cultured with a series of concentrations of SCS was assessed on days 1, 3, and 7. The phenotype polarization of Mφs stimulated by SCS was assessed by flow cytometry (BD Accuri C6) on days 3 and 7.

HUVECs were purchased from the American Type Culture Collection and cultured in DMEM with 10% FBS and 1% penicillin/streptomycin. Mφs and HUVECs were maintained at 37°C in 100% humidified air containing 5% carbon dioxide, with the medium changed every other day.

### Rat aortic ring angiogenesis assay

To simulate the effect of Mφs on endothelial cells in vivo, Mφs were cocultured with aortic ring ex vivo. The aorta was removed from 8-week-old Sprague-Dawley rats and cut into rings 1 to 1.5 mm in width. The manicured aortic rings were placed in starvation medium overnight. Mφs were separately plated on 24-well Transwell insert membranes ($5 \times 10^5$ cells per well) and preincubated in DMEM with 10% FBS overnight to stabilize cell purity and viability. The next day, aortic rings were embedded in 100 μl of neutral rat tail collagen type I and incubated at 37°C for 30 min to allow gelation. Mφs were cocultured in DMEM containing 10% FBS with a series of concentrations of SCS. Medium was first changed on day 3 and then every other day for a week.

### Preparation of conditioned media from Mφs

Mφs were stimulated in DMEM containing 10% FBS with or without SCS (800 ng/ml) for 3 and 7 days, respectively. At the end of induction, cell plates were washed with PBS, and conditioned media were harvested after an additional day of culture with FBS-containing medium. After centrifugation (300*g* for 10 min at 4°C), the conditioned media were stored at −80°C. We used 2% FBS conditioned media for migration experiments and Western blot assay and to detect growth factors. FBS conditioned media (10%) were used for tube formation experiments. In some experiments, we added the VEGF NAbs (1 μg/ml; Santa Cruz Biotechnology, sc7269) or VEGFR2 inhibitors (5 μM; MedChemExpress, SU5408) to the 3-day SCS/Mφs CM.

### RNA analysis by qRT-PCR

To investigate gene expression in Mφs stimulated by SCS, qRT-PCR was performed. Mφs were seeded in six-well plates ($2 \times 10^6$ cells per well) and allowed to adhere and purify overnight. On days 3 and 7, total RNAs were extracted from Mφs with TRIzol reagent. To examine the gene expression in SCS/Mφs CM–stimulated HUVECs, HUVECs were seeded in six-well plates ($2 \times 10^5$ cells per well) and allowed to adhere overnight. Then, the SCS/Mφs CM were added into the plates to incubate for another 1 day, and DMEM with VEGF (2 ng/ml) was used as a positive control. Total RNAs were extracted with TRIzol reagent, followed by a reverse transcription step with PrimeScript RT reagent kit according to the manufacturer's instructions. The qRT-PCR was performed on a CFX96 Touch PCR detection system (Bio-Rad, USA) with a hot start denaturation step at 95°C for 30 s, and then fluorescence intensity was recorded during 40 cycles at 95°C for 5 s and 60°C for 30 s. Murine glyceraldehyde-3-phosphate dehydrogenase (GAPDH) or human GAPDH was used as a housekeeping gene to normalize the expression of the gene of interest depending on the experiment. Relative expression was calculated by comparative $C_t$ ($2^{-\Delta\Delta Ct}$ values indicate fold change of the gene of interest in the samples relative to the Blank; $2^{-\Delta Ct}$ values indicate relative expression of gene of interest between samples normalized to GAPDH). The sequences of primers are listed in tables S1 and S2, respectively.

### Implant supernatant collection

The harvested implants were ground with 500 μl of cold PBS and subsequently centrifuged for 15 min at 300*g* and 4°C to obtain the implant supernatant, which was then stored at −80°C until ELISA assay.

### Quantification of growth factors and cytokines

We performed VEGF or PDGF-BB ELISA analysis of conditioned medium or implant supernatant using a Mouse VEGF Quantikine ELISA kit (Neobioscience) or a Mouse/Rat PDGF-BB Quantikine ELISA kit (R&D Systems). The levels of inflammatory cytokines in conditioned medium were determined using a Proteome Profiler Mouse Cytokine Array kit (R&D Systems). The levels of cytokines of implant supernatant were quantified using a series of ELISA kits (Neobioscience): TNF-α, IL-1β, IL-6, IL-4, IL-10, and TGF-β1. All ELISAs were conducted according to the manufacturers' instructions.

### In vitro assays for migration of HUVECs

A scratch wound healing assay was conducted in 96-well plates to assess the migratory capacity of HUVECs. Briefly, a total of $1 \times 10^4$ RFP (red fluorescent protein)–labeled HUVECs per well were plated overnight and stimulated with a wound in the form of a vertically linear scratch made with a sterile pipette tip. After gently washing twice with PBS to remove cell debris, cells were cultured in the conditioned medium. DMEM with 2% FBS served as a negative control. At 0 and 24 hours after injury, cells were photographed under a fluorescence inverted microscope (Leica). The infiltration area of migrated HUVECs was quantitatively evaluated using ImageJ ($n = 6$).

### In vitro assays for tube formation of HUVECs

Matrigel (Corning) was precoated in 96-well culture plates and incubated at 37°C for 30 min to allow gelation. HUVECs ($2 \times 10^4$ cells per well) were seeded in conditioned medium or control medium on polymerized Matrigel in plates. After incubation for 4 hours, total capillary tube lengths per field were observed and quantified by counting random fields per well with microscopy. Sprouts were defined as a linear extension containing more than one cell.

### Western blot analysis

To explore the effect of Mφs on the signal transduction of VEGFR2 of endothelial cells, we seeded HUVECs on six-well plates in complete medium. Confluent cells were starved (2% FBS) overnight and then stimulated with conditioned media from Mφs for 10 min. Total protein extracts were obtained by lysing cells in cold radioimmunoprecipitation assay (RIPA) buffer containing phenylmethylsulfonyl fluoride (PMSF). The cell lysates were equilibrated with loading buffer to an equal concentration and boiled for 10 min. Subsequently, samples were separated by 8% SDS–polyacrylamide gel electrophoresis (PAGE) at an equal concentration and then blotted on a polyvinylidene fluoride membrane (Millipore). The membranes were incubated with antibodies specific to p-VEGFR2, VEGFR2, p-FAK, FAK, p-Akt, or Akt, followed by incubation with horseradish peroxidase (HRP)–conjugated secondary antibody. GAPDH was used as a loading control.

To investigate the effect of the signal of hypoxia on VEGF expression in vivo, fresh implants retrieved from ischemic mice were immediately lysed using cold RIPA buffer containing PMSF. The cell lysates were equilibrated with loading buffer to an equal concentration and boiled for 10 min. Subsequently, samples were separated by 10% SDS-PAGE at an equal concentration and then blotted on a polyvinylidene fluoride membrane. The membranes were incubated with specific antibodies to HIF-1α, followed by incubation with HRP-conjugated secondary antibody. GAPDH was used as a loading control. Visualization of the protein bands was performed with a chemiluminescence imaging system (Tanon, Shanghai, China). Total intensity of each band was determined with Tanon Image software (version 1.10; Tanon, Shanghai, China).

### Statistical analysis

Results were analyzed using GraphPad Prism software (version 7.0; GraphPad, La Jolla, CA, USA). All data were expressed as means ± SD. *N* numbers indicate biological replicates of experiments performed at least three times unless otherwise indicated. We used unpaired, two-tailed Student's *t* tests for comparisons between two groups. For comparison of multiple experimental groups, either one-way analysis of variance (ANOVA) or two-way ANOVA was performed where indicated. A *P* value of <0.05 was considered statistically significant: $^*P < 0.05$, $^{**}P < 0.01$, $^{***}P < 0.005$, and $^{****}P < 0.001$.

## SUPPLEMENTARY MATERIALS

Supplementary material for this article is available at http://advances.sciencemag.org/cgi/content/full/7/7/eabd8217/DC1

## REFERENCES AND NOTES


1. E. C. Novosel, C. Kleinhans, P. J. Kluger, Vascularization is the key challenge in tissue engineering. *Adv. Drug Deliver. Rev.* **63**, 300–311 (2011).
2. Y.-D. Lin, C.-Y. Luo, Y.-N. Hu, M.-L. Yeh, Y.-C. Hsueh, M.-Y. Chang, D.-C. Tsai, J.-N. Wang, M.-J. Tang, E. I. H. Wei, M. L. Springer, P. C. H. Hsieh, Instructive nanofiber scaffolds with VEGF create a microenvironment for arteriogenesis and cardiac repair. *Sci. Transl. Med.* **4**, 146ra109 (2012).
3. T. Mirabella, J. W. MacArthur, D. Cheng, C. K. Ozaki, Y. J. Woo, M. T. Yang, C. S. Chen, 3D-printed vascular networks direct therapeutic angiogenesis in ischaemia. *Nat. Biomed. Eng.* **1**, 0083 (2017).
4. M. A. Redd, N. Zeinstra, W. Qin, W. Wei, A. Martinson, Y. Wang, R. K. Wang, C. E. Murry, Y. Zheng, Patterned human microvascular grafts enable rapid vascularization and increase perfusion in infarcted rat hearts. *Nat. Commun.* **10**, 584 (2019).

5. H. Karvinen, E. Pasanen, T. T. Rissanen, P. Korpisalo, E. Vaehaekangas, A. Jazwa, M. Giacca, S. Ylä-Herttuala, Long-term VEGF-A expression promotes aberrant angiogenesis and fibrosis in skeletal muscle. *Gene Ther.* **18**, 1166–1172 (2011).
6. R. Z. Lin, C. N. Lee, R. Moreno-Luna, J. Neumeyer, B. Piekarski, P. Zhou, M. A. Moses, M. Sachdev, W. T. Pu, S. Emani, J. M. Melero-Martin, Host non-inflammatory neutrophils mediate the engraftment of bioengineered vascular networks. *Nat. Biomed. Eng.* **1**, 0081 (2017).
7. Committee for Advanced Therapies (CAT); CAT Scientific Secretariat, C. K. Schneider, P. Salmikangas, B. Jilma, B. Flamion, L. R. Todorova, A. Paphitou, I. Haunerova, T. Maimets, J.-H. Trouvin, E. Flory, A. Tsiftsoglou, K. Gudmundsson, M. O'Donovan, G. Migliaccio, J. Ancans, R. Maciulaitis, J.-L. Robert, A. Samuel, J. H. Ovelgoenne, M. Hystad, A. M. Fal, B. S. Lima, A. S. Moraru, P. Turcani, R. Zorec, S. Ruiz, L. Akerblom, G. Narayanan, A. Kent, F. Bignami, J. G. Dickson, D. Niederwieser, M.-A. Figuerola-Santos, I. G. Reischl, C. Beuneu, R. Georgiev, M. Vassiliou, A. Pychova, M. Clausen, T. Methuen, S. Lucas, M. Schussler-Lenz, V. Kokkas, Z. Buzas, N. MacAleenan, M. C. Galli, A. Line, J. Gulbinovic, G. Berchem, M. Fraczek, M. Menezes-Ferreira, N. Vilceanu, M. Hrubisko, P. Marinko, M. Timon, W. Cheng, G. A. Crosbie, N. Meade, M. L. di Paola, T. VandenDriessche, P. Ljungman, L. D'Apote, O. Oliver-Diaz, I. Buettel, P. Celis, Challenges with advanced therapy medicinal products and how to meet them. *Nat. Rev. Drug Discov.* **9**, 195–201 (2010).
8. T. Kinnaird, E. Stabile, M. S. Burnett, M. Shou, C. W. Lee, S. Barr, S. Fuchs, S. E. Epstein, Local delivery of marrow-derived stromal cells augments collateral perfusion through paracrine mechanisms. *Circulation* **109**, 1543–1549 (2004).
9. K. Hu, B. R. Olsen, Osteoblast-derived VEGF regulates osteoblast differentiation and bone formation during bone repair. *J. Clin. Invest.* **126**, 509–526 (2016).
10. H. Xie, Z. Cui, L. Wang, Z. Xia, Y. Hu, L. Xian, C. Li, L. Xie, J. Crane, M. Wan, G. Zhen, Q. Bian, B. Yu, W. Chang, T. Qiu, M. Pickarski, D. Le Thi, J. J. Windle, X. Luo, E. Liao, X. Cao, PDGF-BB secreted by preosteoclasts induces angiogenesis during coupling with osteogenesis. *Nat. Med.* **20**, 1270–1278 (2014).
11. Y. Li, Y. Xiao, C. Liu, The horizon of materiobiology: A perspective on material-guided cell behaviors and tissue engineering. *Chem. Rev.* **117**, 4376–4421 (2017).
12. E. Dondossola, B. M. Holzapfel, S. Alexander, S. Filippini, D. W. Hutmacher, P. Friedl, Examination of the foreign body response to biomaterials by nonlinear intravital microscopy. *Nat. Biomed. Eng.* **1**, 0007 (2017).
13. T. A. Wynn, K. M. Vannella, Macrophages in tissue repair, regeneration, and fibrosis. *Immunity* **44**, 450–462 (2016).
14. P. L. Graney, S. Ben-Shaul, S. Landau, A. Bajpai, B. Singh, J. Eager, A. Cohen, S. Levenberg, K. L. Spiller, Macrophages of diverse phenotypes drive vascularization of engineered tissues. *Sci. Adv.* **6**, eaay6391 (2020).
15. R. L. Jackson, S. J. Busch, A. D. Cardin, Glycosaminoglycans: Molecular properties, protein interactions, and role in physiological processes. *Physiol. Rev.* **71**, 481–539 (1991).
16. I. Capila, R. J. Linhardt, Heparin–protein interactions. *Angew. Chem. Int. Ed.* **41**, 390–412 (2002).
17. L. R. Nih, S. Gojgini, S. T. Carmichael, T. Segura, Dual-function injectable angiogenic biomaterial for the repair of brain tissue following stroke. *Nat. Mater.* **17**, 642–651 (2018).
18. I. Kim, S. S. Lee, S. Bae, H. Lee, N. S. Hwang, Heparin functionalized injectable cryogel with rapid shape-recovery property for neovascularization. *Biomacromolecules* **19**, 2257–2269 (2018).
19. Y. Yu, R. Chen, Y. Sun, Y. Pan, W. Tang, S. Zhang, L. Cao, Y. Yuan, J. Wang, C. Liu, Manipulation of VEGF-induced angiogenesis by 2-N, 6-O-sulfated chitosan. *Acta Biomater.* **71**, 510–521 (2018).
20. A. P. Kusumbe, S. K. Ramasamy, R. H. Adams, Coupling of angiogenesis and osteogenesis by a specific vessel subtype in bone. *Nature* **507**, 323–328 (2014).
21. Y. M. Kolambkar, K. M. Dupont, J. D. Boerckel, H. Nathaniel, D. J. Mooney, D. W. Hutmacher, R. E. Guldberg, An alginate-based hybrid system for growth factor delivery in the functional repair of large bone defects. *Biomaterials* **32**, 65–74 (2011).
22. S. A. Eming, P. Martin, M. Tomic-Canic, Wound repair and regeneration: Mechanisms, signaling, and translation. *Sci. Transl. Med.* **6**, 256sr6 (2014).
23. G. O. Ahn, J. Seita, B.-J. Hong, Y.-E. Kim, S. Bok, C.-J. Lee, K. S. Kim, J. C. Lee, N. J. Leeper, J. P. Cooke, H. J. Kim, I. H. Kim, I. L. Weissman, J. M. Brown, Transcriptional activation of hypoxia-inducible factor-1 (HIF-1) in myeloid cells promotes angiogenesis through VEGF and S100A8. *Proc. Natl. Acad. Sci. U.S.A.* **111**, 2698–2703 (2014).
24. M. Bartneck, C. T. Schlößer, M. Barz, R. Zentel, C. Trautwein, T. Lammers, F. Tacke, Immunomodulatory therapy of inflammatory liver disease using selectin-binding glycopolymers. *ACS Nano* **11**, 9689–9700 (2017).
25. A. Sica, V. Bronte, Altered macrophage differentiation and immune dysfunction in tumor development. *J. Clin. Invest.* **117**, 1155–1166 (2007).
26. T. A. Wynn, A. Chawla, J. W. Pollard, Macrophage biology in development, homeostasis and disease. *Nature* **496**, 445–455 (2013).
27. P. J. Murray, T. A. Wynn, Protective and pathogenic functions of macrophage subsets. *Nat. Rev. Immunol.* **11**, 723–737 (2011).
28. H. G. Augustin, G. Y. Koh, Organotypic vasculature: From descriptive heterogeneity to functional pathophysiology. *Science* **357**, eaal2379 (2017).
29. F. O. Martinez, S. Gordon, The M1 and M2 paradigm of macrophage activation: Time for reassessment. *F1000Prime Rep.* **6**, 13 (2014).
30. H. H. He, J. Y. Xu, C. M. Warren, D. Duan, X. M. Li, L. L. Wu, M. L. Iruela-Arispe, Endothelial cells provide an instructive niche for the differentiation and functional polarization of M2-like macrophages. *Blood* **120**, 3152–3162 (2012).
31. K. Krishnasamy, A. Limbourg, T. Kapanadze, J. Gamrekelashvili, C. Beger, C. Häger, V. J. Lozanovski, C. S. Falk, L. C. Napp, J. Bauersachs, Blood vessel control of macrophage maturation promotes arteriogenesis in ischemia. *Nat. Commun.* **8**, 952 (2017).
32. E. M. Bekes, B. Schweighofer, T. A. Kupriyanova, E. Zajac, V. C. Ardi, J. P. Quigley, E. I. Deryugina, Tumor-recruited neutrophils and neutrophil TIMP-free MMP-9 regulate coordinately the levels of tumor angiogenesis and efficiency of malignant cell intravasation. *Am. J. Pathol.* **179**, 1455–1470 (2011).
33. S. Reimann, D. Gröger, C. Kuehne, S. B. Riese, J. Dernedde, R. Haag, Shell cleavable dendritic polyglycerol sulfates show high anti-inflammatory properties by inhibiting L-selectin binding and complement activation. *Adv. Healthc. Mater.* **4**, 2154–2162 (2015).
34. E. Young, The anti-inflammatory effects of heparin and related compounds. *Thromb. Res.* **122**, 743–752 (2008).
35. N. S. Gandhi, R. L. Mancera, The structure of glycosaminoglycans and their interactions with proteins. *Chem. Biol. Drug Des.* **72**, 455–482 (2008).
36. K. L. Christman, V. Vazquez-Dorbatt, E. Schopf, C. M. Kolodziej, R. C. Li, R. M. Broyer, Y. Chen, H. D. Maynard, Nanoscale growth factor patterns by immobilization on a heparin-mimicking polymer. *J. Am. Chem. Soc.* **130**, 16585–16591 (2008).
37. B. Richard, R. Swanson, S. T. Olson, The signature 3-O-sulfo group of the anticoagulant heparin sequence is critical for heparin binding to antithrombin but is not required for allosteric activation. *J. Biol. Chem.* **284**, 27054–27064 (2009).
38. T. Wang, Y. Zhou, W. Xie, L. Chen, H. Zheng, L. Fan, Preparation and anticoagulant activity of N-succinyl chitosan sulfates. *Int. J. Biol. Macromol.* **51**, 808–814 (2012).
39. H. Chen, Y. Yu, C. Wang, J. Wang, C. Liu, The regulatory role of sulfated polysaccharides in facilitating rhBMP-2-induced osteogenesis. *Biomater. Sci.* **7**, 4375–4387 (2019).
40. Y. Yu, J. Chen, R. Chen, L. Cao, W. Tang, D. Lin, J. Wang, C. Liu, Enhancement of VEGF-mediated angiogenesis by 2-*N*,6-*O*-sulfated chitosan-coated hierarchical PLGA scaffolds. *ACS Appl. Mater. Interfaces* **7**, 9982–9990 (2015).
41. A. P. Kusumbe, S. K. Ramasamy, A. Starsichova, R. H. Adams, Sample preparation for high-resolution 3D confocal imaging of mouse skeletal tissue. *Nat. Protoc.* **10**, 1904–1914 (2015).



**Acknowledgments**

**Funding:** This research was supported by the National Natural Science Foundation of China for Innovative Research Groups (no. 51621002) and the National Natural Science Foundation of China (no. 31870953). This study was also supported by the 111 Project (B14018). **Author contributions:** Y. Yu conceived the ideas for experimental designs, executed the majority of the experiments, analyzed data, and wrote the manuscript. K.D. provided technical assistance with flow cytometry and participated in experimental design. Z.G. and T.S. assisted with animal surgery. W.T. and Y. Yuan critically reviewed the manuscript and participated in discussing data interpretation. J.W. and C.L. supervised the project, conceived the ideas, and finalized the manuscript. **Competing interests:** The authors declare that they have no competing interests. **Data and materials availability:** All data needed to evaluate the conclusions in the paper are present in the paper and/or the Supplementary Materials. Additional data related to this paper may be requested from the authors.

Submitted 14 July 2020
Accepted 21 December 2020
Published 10 February 2021
10.1126/sciadv.abd8217

**Citation:** Y. Yu, K. Dai, Z. Gao, W. Tang, T. Shen, Y. Yuan, J. Wang, C. Liu, Sulfated polysaccharide directs therapeutic angiogenesis via endogenous VEGF secretion of macrophages. *Sci. Adv.* **7**, eabd8217 (2021).